

# Structure of Sick Cell Hemoglobin Fibers Probed with UV Resonance Raman Spectroscopy<sup>†</sup>

Liliana Sokolov and Ishita Mukerji\*

Molecular Biology and Biochemistry Department, Molecular Biophysics Program, Wesleyan University, Middletown, Connecticut 06459-0175

Received: February 7, 2000; In Final Form: May 22, 2000

The structure of sickle cell hemoglobin (Hb S) ( $\beta 6$  Glu  $\rightarrow$  Val) fibers was probed using UV resonance Raman (UVR) spectroscopy. For these studies a functional analogue of Hb S, fluoromet Hb S, was used to study structural changes that accompany fiber formation. The amide backbone and aromatic residues of Hb S were selectively investigated using excitation wavelengths of 210, 215, and 230 nm. In the 210 and 215 nm excited fiber spectra, the intensity of all Phe bands increases dramatically. At the excitation wavelengths used, the Phe signal intensity reflects the local environment and increases linearly with increasing ethylene glycol concentration. Thus, UVR fiber spectra are suggestive of an increase in hydrophobicity of the Phe local environment, which results from the formation of lateral and axial fiber contacts that are primarily nonpolar and hydrophobic in nature. The observed UVR signal is assigned to the  $\beta_1 85$  Phe residue, which, together with the  $\beta_1 88$  Leu residue, forms a hydrophobic lateral contact with the mutated  $\beta_2 6$  residue. In addition, 230 nm difference spectra are suggestive that H-bonds stabilizing the  $\alpha_1 \beta_2$  interface are stronger in fibers than in unassociated T-state tetramers. The W3 mode in fiber difference spectra occurs at 1550 and 1565  $\text{cm}^{-1}$ , indicative of an increase in Trp spectral heterogeneity. The +6  $\text{cm}^{-1}$  upshift of the W3 mode is attributed to increased hydrophobicity of Trp local environment and is assigned to the  $\beta_2 15$  Trp residue. Other structural changes include an increase in disorder upon fiber formation, as shown by the frequencies of protein backbone amide vibrational modes. UVR spectroscopic results are consistent with the structural details of the Hb S double strand observed crystallographically and provide new information regarding local environment and strength of H-bond interactions.

## Introduction

In sickle cell hemoglobin, a single-residue mutation in the  $\beta$  subunits ( $\beta 6$  Glu  $\rightarrow$  Val) drives the association of individual tetramers into long fibers. During fiber formation, the  $\beta 6$  Val residue interacts with a hydrophobic pocket formed by the  $\beta 85$  Phe and  $\beta 88$  Leu residues on a different tetramer. This “donor–acceptor” interaction, in which  $\beta 6$  Val is donated to the EF acceptor pocket, requires the deoxy or T-allosteric state, as exposure of the acceptor pocket only occurs in this state<sup>1–3</sup> (Figure 1). Hb S fiber structure has been studied using electron microscopy,<sup>4–6</sup> X-ray crystallography,<sup>1,2,7</sup> and light scattering.<sup>8,9</sup> X-ray crystallography has revealed that the basic architecture of the fibers is the assembly of hemoglobin molecules into double strands. These strands are stabilized by intermolecular axial and lateral contacts, particularly lateral contacts involving the mutated  $\beta 6$  Val residue.<sup>7,10</sup> Although structural differences exist between crystalline fibers and Hb S gels, the structure of Hb S fibers is generally thought to be the Wishner–Love double strand observed in the crystal with a slight helical twist. Intermolecular contacts predicted from the crystal structure have been verified in copolymerization studies of Hb S mutants<sup>11,12</sup> and demonstrate the relevance of the double-strand model.

In this study, we have compared the structure of sickle cell fibers to HbS tetramers using UV resonance Raman (UVR) spectroscopy. Previous studies have shown that UVR spec-

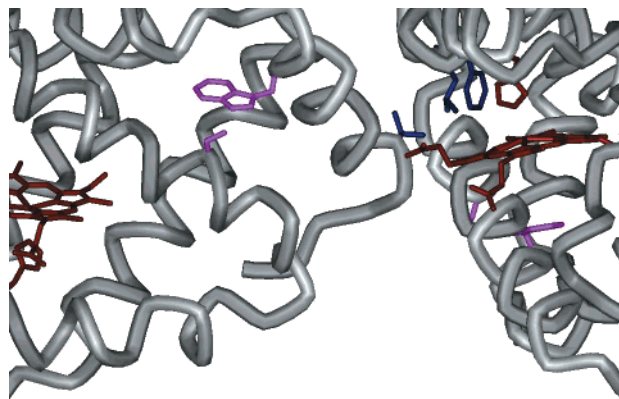


**Figure 1.** Schematic diagram of the  $^2\beta_2$  donor– $^1\beta_1$  acceptor interaction. The residues that form the donor–acceptor interaction,  $^2\beta_2 6$  Val,  $^1\beta_1 88$  Leu, and  $^1\beta_1 85$  Phe, are shown in dark blue. Heme groups with coordinating  $\beta 92$  His residues are shown in dark red. The  $\beta 15$  Trp... $\beta 72$  Ser H-bond is shown in pink. The diagram was made using WebLab ViewerLite and the coordinates from the deoxy Hb S X-ray crystal structure (2HBS.PDB).

troscopy is sensitive to changes in both quaternary<sup>13–16</sup> and tertiary structure<sup>17–19</sup> of hemoglobin as it undergoes the allosteric transition. In particular, spectral features characteristic of the R to T transition have been identified and attributed to the formation of stabilizing H-bonds across the  $\alpha_1 \beta_2$  and the symmetry related  $\alpha_2 \beta_1$  interface in the T-state<sup>13</sup> (Figure 2). Previous UVR and fluorescence spectroscopic experiments of

<sup>†</sup> Part of the special issue “Thomas Spiro Festschrift”.

\* To whom correspondence should be addressed. Phone: 860-685-2422. Fax: 860-685-2141. E-mail: imukerji@wesleyan.edu.

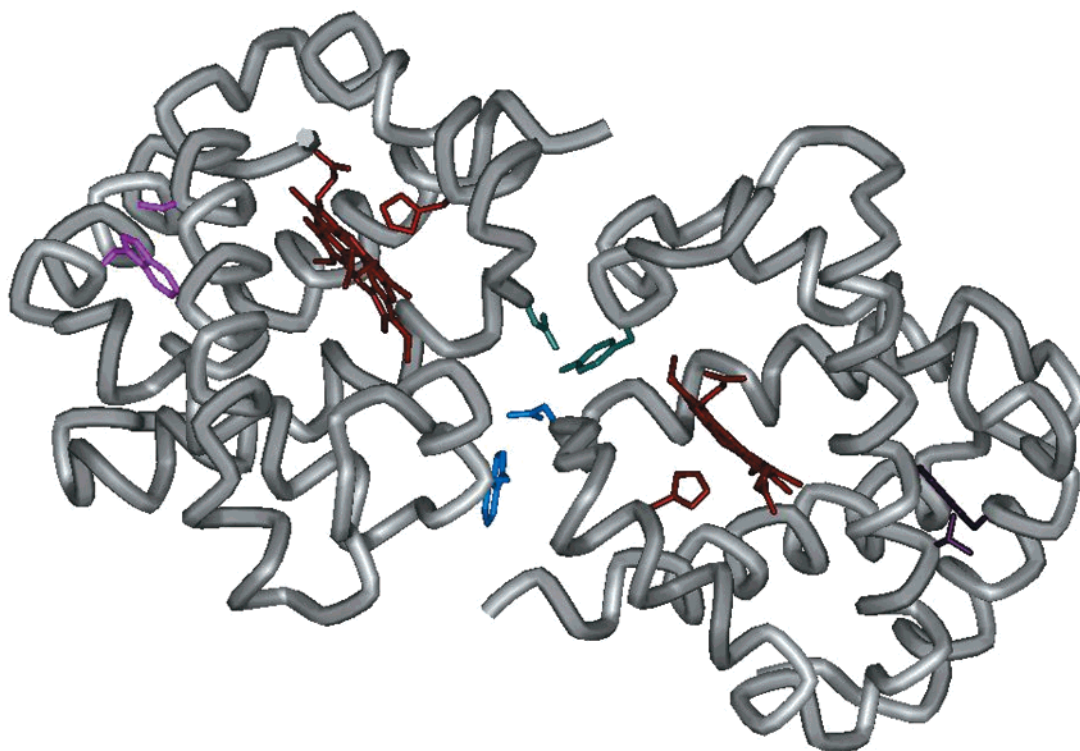


**Figure 2.** Schematic diagram of the  $\alpha_1\beta_2$  interaction. The residues forming the intersubunit H-bonds ( $\beta 37$  Trp $\cdots\alpha 94$  Asp) and ( $\alpha 42$  Tyr $\cdots\beta 99$  Asp) are shown in blue and green, respectively. Heme groups with coordinating His residues are shown in dark red. Residues that form an H-bond between the A and E helices of one subunit,  $\beta 15$  Trp $\cdots\beta 72$  Ser, and the symmetry-related  $\alpha 14$  Trp $\cdots\alpha 67$  Thr are shown in pink and dark purple, respectively. The diagram was made as in Figure 1.

Hb S tetramers demonstrated that the tertiary structure of Hb S differs from that of Hb A. These studies showed that the interior symmetry-related Trp residues,  $\alpha 14$  and  $\beta 15$ , form stronger H-bonds with their respective partners on the E-helices, indicative of a displacement of the A-helix.<sup>20,21</sup> This finding is consistent with the most recent X-ray crystal structure of deoxyhemoglobin S, in which the A-helix of only the donor  $\beta$  subunits ( $\beta_1$  are mutant valine acceptor subunits and  $\beta_2$  are mutant valine donor subunits) was observed to be displaced toward the protein interior.<sup>7</sup>

These studies employ the fluoromet derivative of Hb S (FmetHb S), which adopts the T-quaternary state in the presence of the allosteric effector, inositol hexaphosphate (IHP).<sup>17,20,22</sup> Electron microscopy and turbidity measurements have demonstrated that this derivative forms fibers similar to those of deoxy Hb S.<sup>23</sup> Polymerization of Hb S depends on many factors, including protein concentration and ionic strength of the solution. Unassociated T-state tetramers are studied at the same protein concentration as FmetHb S fibers, through modulation of solution ionic strength. Thus, in this study we compare the protein in three distinct states: the R-quaternary state, the T-quaternary state, and the polymerized state (F-state).

Polymerization studies using engineered Hb S mutants, in which  $\beta 85$  Phe and  $\beta 88$  Leu have been mutated to Glu and Ala, have shown that hydrophobicity and steric constraints of the donor–acceptor interaction are important factors in the polymerization process<sup>24–28</sup> (Figure 1). In the current investigation the relative hydrophobicity of the acceptor pocket is directly monitored through the  $\beta 85$  Phe residue. It has been previously demonstrated<sup>29</sup> and further investigated by us (present work) that the intensity of the Phe signal is sensitive to the local environment, in which Phe signal intensity scales with hydrophobicity. We have employed this sensitivity of the UVRR signal to the local environment to probe the  ${}^2\beta_2$  donor– ${}^1\beta_1$

acceptor interaction. In these studies, which compare the UVRR signal from fibers with that of unassociated tetramers in both allosteric states, an increase in signal intensity is observed for all Phe Raman bands in fibers relative to the tetramers. Thus, these studies directly show the increased hydrophobicity of Phe residues in Hb S fibers, as predicted from X-ray crystallographic characterization of the donor–acceptor interaction. In addition, these studies also examine the quaternary structure of tetramers in the fibers and are suggestive of stronger  $\alpha_1\beta_2$  intersubunit contacts, as monitored by the  $\beta 37$  Trp $\cdots\alpha 94$  Asp and  $\alpha 42$  Tyr $\cdots\beta 99$  Asp H-bonds (Figure 2). The increased strength of these quaternary H-bonds potentially accounts in part for the slower ligand binding rate<sup>30</sup> and lower ligand affinity<sup>31</sup> observed for Hb S fibers relative to T-state tetramers. These studies also probe secondary structure conformation through amide vibrational modes and Trp local environment. The results are discussed within the context of the proposed fiber structure and crystalline double strands.

## Materials and Methods

**Sample Preparation.** Hb S was isolated from the blood of AS and SS patients following standard procedures<sup>32</sup> and further purified on a Whatman DE-52 column by gradient elution from 50 mM Tris–acetate, pH 8.3, to 50 mM Tris–acetate, pH 7.3.<sup>33</sup> Hb S was converted to the fluoromet (Fmet) form following the procedure of Jayaraman et al.<sup>17</sup> The concentration of fluoromethemoglobin (FmetHb S) was determined spectrophotometrically, using the heme extinction coefficients of  $\epsilon_{606} = 10.3 \text{ mM}^{-1}\text{cm}^{-1}$  and  $\epsilon_{490} = 10.9 \text{ mM}^{-1}\text{cm}^{-1}$ .<sup>34</sup>

FmetHb S samples for UVRR experiments contained 1.2 mM FmetHb S, 0.3 M sodium fluoride, and 0.5 M phosphate buffer, pH 6.5. Formation of unassociated T-state tetramers was accomplished by the addition of a 20-fold excess of inositol

hexaphosphate (IHP)/tetramer. Fiber formation was induced by increasing the IHP concentration to 140 mM. Fiber formation was confirmed by monitoring sample turbidity at 700 nm as a function of time.<sup>23</sup>

**UV Resonance Raman Spectroscopy.** A Nd:YLF-pumped Ti:Sapphire laser system (Quantronix, New York) was used to generate all the excitation wavelengths by frequency quadrupling the fundamental output of the Ti:Sapphire laser with two barium borate (BBO) crystals. The laser system has been described elsewhere.<sup>20,35</sup> The system was operated at a repetition rate of 1–1.5 kHz and an average power of 0.8 mW. Data were calibrated with acetone and ethanol and are accurate to  $\pm 1 \text{ cm}^{-1}$ ; relative shifts are accurate to  $\pm 0.25 \text{ cm}^{-1}$ . Spectra shown result from a total of 3 h of summed spectra. For tetramers, the acquisition time for each spectrum was 1 h, and for fibers, the acquisition time for each spectrum was 15 min. Samples were contained in a metal disk with a quartz circular coverslip and were spun continuously. Tetramer samples were cooled with  $\text{N}_2$  gas that had passed through a dry ice/2-propanol bath. Fiber data were collected at room temperature. Data were normalized to unity at  $2020 \text{ cm}^{-1}$ , and all difference spectra were generated using a factor of 1. We established that this band does not shift in frequency or increase in intensity upon formation of fibers or the T-state, by using the internal intensity and frequency standard  $\text{NaClO}_4$ . Data manipulation and analysis were done using the Labcalc and Grams/32 (Galactic Industries, NH) programs.

The Raman excitation profiles were obtained using solutions containing 1 mM Phe and 0.2 M  $\text{NaClO}_4$ . Each spectrum was acquired for 15 min. Raman cross sections were calculated using the following equation:  $\sigma_n = \sigma_s(I_n/I_s)(C_s/C_n)[(\nu_0 - \nu_s)/(\nu_0 - \nu_n)]^4$  where  $I$  is the peak height intensity of the standard ( $s$ ) and of the band of interest ( $n$ ),  $C$  is the molar concentration of the standard and the sample, respectively, and  $\nu_0$  is the excitation frequency.<sup>35</sup> Solutions of 2 mM Phe with 0.2 M  $\text{NaClO}_4$  in a 0.05 M sodium phosphate buffer, pH 7.0, were used to obtain spectra in the presence of increasing concentrations of ethylene glycol (v/v). Ethylene glycol concentrations (v/v) ranging from 0 to 70% were studied. Each spectrum was acquired for 15 min.

## Results and Discussion

**UVRR Investigation of Trp and Tyr Residues: Probing the  $\alpha_1\beta_2$  Interface.** UVRR spectra obtained with an excitation wavelength of 230 nm primarily result from Tyr and Trp residues, where the relative contribution of Phe residues is low.<sup>13</sup> In the fibers and R-state spectra shown in Figure 3, all of the modes have been previously assigned<sup>13</sup> and arise from the 6 Tyr and 3 Trp residues present per  $\alpha\beta$  dimer. This study employs the fluoromet derivative of Hb S (FmetHb S), in which the heme Fe is oxidized ( $\text{Fe}^{2+} \rightarrow \text{Fe}^{3+}$ ) and the sixth ligand position is occupied by a fluoride ion. In this derivative, formation of the T-state is induced by addition of the allosteric effector, inositol hexaphosphate (IHP). The difference spectrum shown in Figure 3d is characteristic of the R to T transition, and it has been shown previously that FmetHb S with and without IHP yields the same quaternary difference features as Hb A.<sup>17, 20</sup>

**$\alpha 42$  Tyr Residue.** In the region above  $1500 \text{ cm}^{-1}$  a double sigmoidal feature is observed that can be attributed to the Y8a and Y8b modes of Tyr (Figure 3d). This feature results from a frequency upshift of these Tyr bands upon formation of the T-state. On the basis of their analysis of the deoxy and oxy Hb A X-ray crystal structures, Spiro and co-workers<sup>13</sup> assigned this feature to the  $\alpha 42$  Tyr, since it is the only Tyr residue which experiences a significant change in H-bonding upon formation

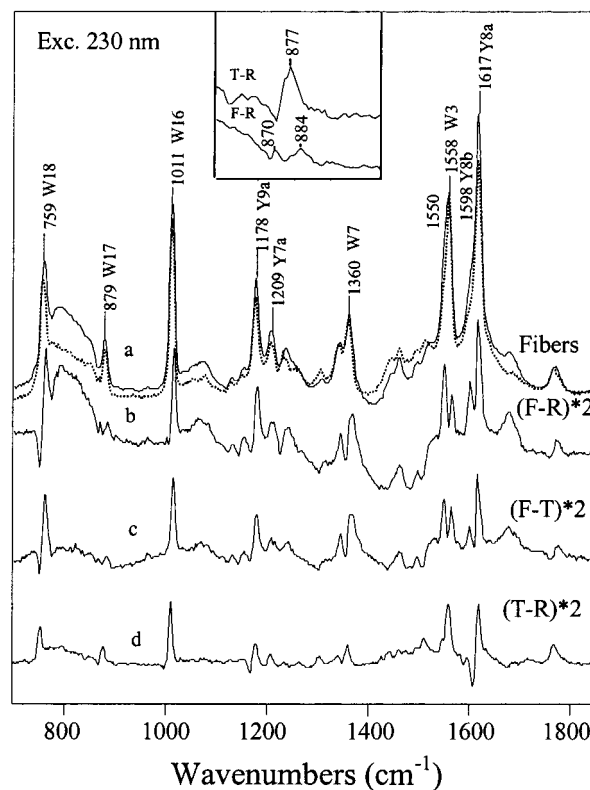


**Figure 3.** (a) 230 nm-excited UVRR spectra of FmetHb S fibers and R-state tetramers. (b) Difference spectrum generated between fibers and R-state tetramers (F–R). (c) Difference spectrum generated between fibers and T-state tetramers (F–T). (d) Difference spectrum generated between T-state and R-state tetramers (T–R). The inset depicts the W17 band ( $850\text{--}920 \text{ cm}^{-1}$ ) in the T–R (top) and F–R (bottom) difference spectra. All spectra were obtained with 230 nm excitation.

of the T-state. This residue has no H-bond partner in the R-state but forms a critical intersubunit H-bond to the  $\beta 99$  Asp residue in the T-state. UVRR studies of isotope labeled,<sup>36</sup> mutant,<sup>19,37</sup> and modified<sup>37,38</sup> Hb molecules have confirmed that the observed frequency shift arises from Tyr residues contained in the  $\alpha$  chains. The observed frequency *upshift* was interpreted to be indicative of the  $\alpha 42$  Tyr acting as an H-bond acceptor.<sup>13</sup> However, more recent FTIR experiments of isotopically labeled recombinant Hb<sup>39</sup> argue against protonation of the  $\beta 99$  Asp residue at neutral pH and are indicative of the Tyr residue acting as an H-bond donor. The frequency upshift of the Tyr Y8a and Y8b modes was attributed to compensating H-bond formation and positive polarization from nearby residues, which override the expected frequency downshifts from donor H-bond formation.<sup>39</sup>

In the difference spectrum generated between fibers and R-state tetramers, positive peaks are observed for Y8a and Y8b and the derivative shape is not as pronounced (Figure 3b). Nevertheless, a comparison of the parent spectra (Figure 4) reveals that Y8a is shifted by  $+2.1 \text{ cm}^{-1}$  in the polymerized state (F) relative to R-state tetramers. This frequency shift is in the same direction as that in the T–R spectra; however, it is of greater magnitude ( $+2.1$  vs  $+1.2 \text{ cm}^{-1}$ ). The absence of a derivative shape in the difference spectra reflects the stronger intensity of Raman bands in the fiber spectra relative to tetramers (Figure 3). Concomitantly larger frequency shifts are also observed for other Tyr modes in the spectrum, namely Y7a and Y9a, occurring at approximately 1209 and  $1177 \text{ cm}^{-1}$ , respectively (Table 1). The largest frequency shift is observed in the polymerized state, and the magnitude of the shift observed for

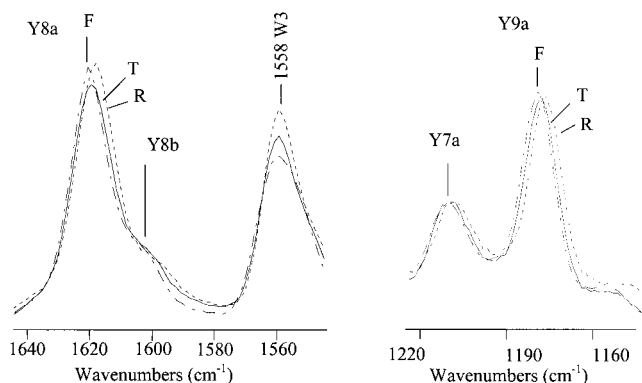


**Figure 4.** Expanded view of the Y7a, Y9a (1050–1250  $\text{cm}^{-1}$ ) and Y8a, Y8b (1500–1650  $\text{cm}^{-1}$ ) regions of the spectrum for fibers (---) and T-state (—) and R-state (- - -) tetramers. Original spectra are shown in Figure 3. Frequencies and relative frequency shifts are reported in Table 1.

**TABLE 1: Frequency of Tyr Modes in UVR R Spectra of Fibers and Tetramers and Associated Difference Spectra**

	Y8a	Y7a	Y9a
	Frequency ( $\text{cm}^{-1}$ )		
fibers	1617.8	1208.8	1175.5
T-state	1616.9	1207.8	1176.4
R-state	1615.7	1206.8	1175.5
	Frequency Shift ( $\Delta \text{cm}^{-1}$ )		
T–R	1.2	1.0	0.9
F–R	2.1	2.0	1.7
F–T	0.9	1.0	1.1

fibers relative to the T-state is comparable to the frequency shift of the T-state relative to the R-state. The similarity in shift magnitude implies that the interaction is strengthened by approximately the same amount for fiber formation as for T-state formation (Table 1). Although UVR R experiments of Hb Rouen (Y $\alpha$ 140H) are suggestive that Tyr  $\alpha$ 140 also contributes to the observed frequency shift,<sup>37</sup> examination of the X-ray crystal structure of deoxy Hb S does not reveal a significantly different environment for the  $\alpha$ 140 residue relative to deoxy Hb A.<sup>7,40</sup> Thus, the observed frequency shift is attributed primarily to the intersubunit H-bond formed by the  $\alpha$ 42 Tyr residue, although a minor contribution from the  $\alpha$ 140 Tyr cannot be ruled out.

The direction of the frequency shift is contrary to that expected for a donor H-bond, which is predicted from the X-ray crystal structure of deoxy HbA<sup>40</sup> and recent experiments.<sup>39</sup> We suggest that, similar to the T-state, a stronger H-bonding interaction between the  $\alpha$ 42 Tyr and the  $\beta$ 99 Asp residues in the fibers coupled with the compensating H-bond from the Asp  $\beta$ 94 backbone NH and the charged environment of the  $\beta$ 40 Arg leads to the positive frequency shift.<sup>39</sup>

**Trp Residues:  $\beta$ 37.** In the parent spectra (Figure 3), one of the strongest peaks observed is the W3 Trp mode at 1558  $\text{cm}^{-1}$ . This band, which mainly involves  $\text{C}_2\text{--C}_3$  stretching vibrations, is heterogeneous because of the dependence of this vibration on the  $\chi^2$  torsion angle about the  $\text{C}_\alpha\text{--C}_\beta\text{--C}_3\text{--C}_2$  linkage.<sup>41</sup> In earlier studies using the mutant Hb Rothschild (W $\beta$ 37R), the shoulder at 1550  $\text{cm}^{-1}$  was assigned to the  $\beta$ 37 Trp, while the symmetry-related  $\alpha$ 14 and  $\beta$ 15 Trp residues gave rise to the main band at 1558  $\text{cm}^{-1}$ .<sup>13</sup> In Hb S, the W3 mode is more intense relative to Hb A, and the increase in intensity was attributed to a strengthening of the  $\beta$ 15Trp $\cdots\beta$ 72 Ser H-bond.<sup>20,21</sup> The H-bond strengthening detected spectroscopically is consistent with the A-helical displacement observed in donor  $\beta$  subunits by X-ray crystallography.<sup>7</sup>

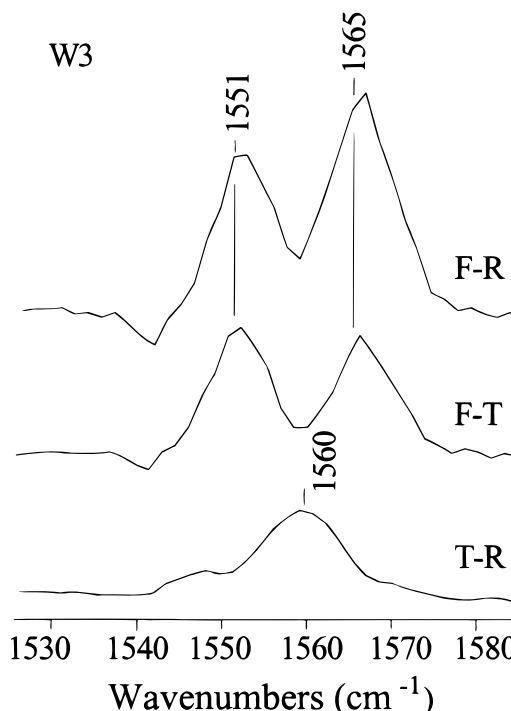


**Figure 5.** Expansion of the Trp W3 region (1520–1600  $\text{cm}^{-1}$ ) from the 230 nm- excited F–R (top), F–T (middle), and T–R (bottom) difference spectra shown in Figure 3.

In the T–R difference spectrum, the W3 shoulder in the parent spectra emerges as a resolvable peak and reflects the formation of the  $\beta$ 37 Trp $\cdots\alpha$ 94 Asp H-bond. In the FmetHb S difference spectrum, an additional peak is observed at 1560  $\text{cm}^{-1}$ , which has been assigned to the interior Trp residues,  $\alpha$ 14 and  $\beta$ 15. This band, which is not observed in unmodified Hb A, results from stronger H-bonding at these Trp residues and arises from the presence of fluoride ligands in the T-state.<sup>17</sup> In difference spectra generated between fibers and the T- and R-states (Figure 3b, c), the W3 mode appears as two resolvable bands at 1551 and 1565  $\text{cm}^{-1}$ . As for the T-state, the peak observed in the F–R difference spectrum at 1551  $\text{cm}^{-1}$  is attributed to the formation of the  $\beta$ 37 Trp $\cdots\alpha$ 94 Asp H-bond. The F–T difference spectrum (Figure 5) demonstrates that the intensity of this band is greater in the fibers. Increases in H-bond strength and/or hydrophobicity lead to a red-shifting of the Raman excitation profile and a subsequent increase in the intensity of Trp bands using 230 nm excitation.<sup>13</sup> Therefore, the 1551  $\text{cm}^{-1}$  peak observed in the F–T difference spectrum is suggestive of a stronger H-bond interaction between the  $\beta$ 37 Trp and  $\alpha$ 94 Asp residues in Hb S fibers relative to unassociated T-state tetramers.

The increased strength of the H-bond interaction is further supported by the W17 mode in both the F–T and the F–R difference spectra, which appears as two bands at 885 and 870  $\text{cm}^{-1}$  (Figure 3, inset). The frequency of the W17 mode, which is a mixture of ring breathing and  $\text{N}_1\text{H}$  motions, is sensitive to the environment and to H-bonding at the indole ring nitrogen. The mode downshifts in proton-acceptor solvents and appears at higher frequencies in nonpolar solvents, such as  $\text{CS}_2$  and cyclohexane.<sup>42</sup> The peak observed at 870  $\text{cm}^{-1}$  is indicative of a strongly H-bonded Trp<sup>42</sup>, and we suggest that the  $\beta$ 37 Trp residue gives rise to the observed peak at 870  $\text{cm}^{-1}$  (Figure 3, inset). The significant downshift of this band detected in Hb S fibers results from an increase in strength of the H-bond formed between the  $\beta$ 37 Trp and the  $\alpha$ 94 Asp residues.

**TABLE 2: Intensity Ratio of the Trp W7 Band in UVRR Spectra of Fibers and Tetramers and Associated Difference Spectra**

	intensity ratio $I_{1360}/I_{1340}$
fibers	2.7
T-state	2.5
R-state	2.2
T-R	2.6
F-R	2.1
F-T	2.2

**UVRR Spectroscopy of Trp Residues: Probing Local Environment and Tertiary Structure.** The increased hydrophobicity of Trp local environment, as indicated by the 884  $\text{cm}^{-1}$  W17 band (see above), leads to an intensity increase of other Trp bands in the fiber spectra (Figure 3). Interestingly, even the weakest Trp modes in the 230 nm-excited spectra, W4 (1495  $\text{cm}^{-1}$ ) and W6 (1446  $\text{cm}^{-1}$ ), are observable in the difference spectra. This intensity increase can be related to the red-shift of the Raman excitation profile that results from an increase in hydrophobicity and/or strength of H-bonding. Further indication of the increased hydrophobicity can be derived from the relative intensity ratio of the W7 doublet at 1340 and 1360  $\text{cm}^{-1}$ , which has been previously shown to be a sensitive marker of environment.<sup>43–45</sup> The  $I_{1360}/I_{1340}$  ratio increases from 2.2 in the R-state to 2.5 in the T-state and 2.7 in the fiber or F-state, reflecting a steady increase in hydrophobicity. This increase is mirrored in the difference spectra in which the largest ratio (2.6) is observed in the F-R difference spectrum, and the F-T and T-R difference spectra both exhibit ratios of approximately 2.1 (Table 2).

We note that the W7 doublet occurs at higher frequencies in the F-T and F-R difference spectra (1344 and 1365  $\text{cm}^{-1}$ ) relative to the parent and the T-R difference spectra (1340 and 1360  $\text{cm}^{-1}$ ) (Figure 3). This mode is unusually complex and is usually observed as a doublet, a consequence of Fermi resonance of the W7 fundamental with two combinations of out-of-plane vibrations (W25 + W33 and W28 + W29). In a previous study of bacteriorhodopsin, the W7 mode was observed as a triplet with one band occurring at 1370  $\text{cm}^{-1}$ . The upshift of the combination band was attributed to steric interactions of the indole ring with the 9-methyl and 13-methyl groups of the retinal.<sup>46</sup> In this study, both modes of the W7 doublet are observed to shift to higher frequency. Thus, given the structure of Hb and the type of shift observed, we suggest that the increased hydrophobic environment leads to the wavenumber shift. H-bonding of the  $\beta 37$  Trp residue is not considered to be the source of the W7 frequency shift, as a similarly strongly H-bonded Trp in lysozyme did not exhibit any anomalous frequency shifts of the W7 doublet.<sup>42</sup>

**Trp Residues:  $\beta 15$ .** We suggest that the Trp residue, which experiences the greatest change in local environment as a consequence of fiber formation, is the  $\beta 15$  Trp residue located on the A-helix (Figure 1). In the X-ray crystal structure, the A-helix of the donor  $\beta$  subunits was displaced toward the interior of the protein to a greater extent than in the acceptor  $\beta$  subunits or deoxy Hb A.<sup>7</sup> This perturbation of the tertiary structure was detected in UVRR spectra of unassociated Hb S tetramers as an increase in band intensity at 1559  $\text{cm}^{-1}$  and was attributed to a strengthening of the  $\beta 15$  Trp... $\beta 72$  Ser H-bond. In the F-T and F-R difference spectra, the W3 mode exhibits an increase in signal intensity and frequency (Figure 5). In the fibers' difference spectra, the higher frequency component of the W3 band occurs at 1565  $\text{cm}^{-1}$ , which is upshifted by +6  $\text{cm}^{-1}$  relative to the parent and T-R difference spectra. This mode

**TABLE 3: Frequency of Trp Residues in the W3 Envelope**

Trp residue	frequency ( $\text{cm}^{-1}$ )			torsion angle <sup>d</sup>
	predicted <sup>a</sup>	detected <sup>b</sup>	fitted <sup>c</sup>	
$\beta 37$	1551	1551.4	1549.2	96.25
$\alpha 14$	1554	1558	1558.2	103.45
$\beta_1 15$	1553.3	1558	1557.7	101.9
$\beta_2 15$	1556.7	1565	1564.2	115.85

<sup>a</sup> Predicted frequencies as calculated from the empirical relationship of Miura and co-workers.<sup>41</sup> <sup>b</sup> Experimentally observed frequencies, taken from data shown in Figure 3. <sup>c</sup> Fitted frequencies obtained by fitting the W3 envelope from 1530 to 1570  $\text{cm}^{-1}$  with Lorentzian peaks using three bands for fibers and two bands for the R-state. Optimization of the fit was judged by visual inspection and the  $\chi^2$  value. <sup>d</sup> Trp  $C_\alpha-C_\beta-C_2-C_3$  torsion angle measured using the coordinates from the X-ray crystal structure of deoxy Hb S.<sup>7</sup>

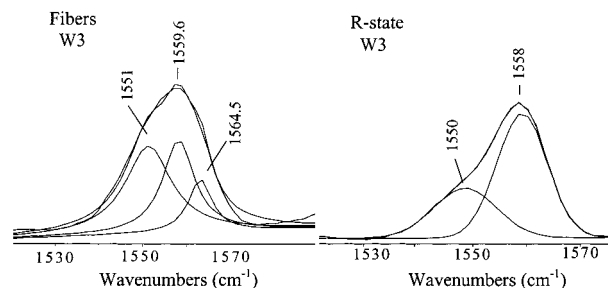


**Figure 6.** Expansion of the Trp W3 region (1520–1600  $\text{cm}^{-1}$ ) of the FmetHb S fibers' (left) and R-state tetramers' (right) spectra in Figure 3. The W3 band reflects the heterogeneity of the Trp population. The W3 band of R-state tetramers is well-described by two peaks, while the W3 band of FmetHb S fibers requires three peaks. Smooth curves result from curve fitting, and the frequencies are reported in Table 3.

is sensitive to side chain conformation and the angle that the indole ring makes with the protein backbone as measured by the  $\chi^2$  torsional angle. The torsion angle of the  $\beta 15$  Trp residues located on donor subunits is 10–15° higher than that observed for  $\beta 15$  Trp residues in acceptor  $\beta$  subunits or the symmetry related  $\alpha 14$  Trp residues, as revealed by the X-ray crystal structure data<sup>7</sup> (Table 3). Thus, the structural data predict three classes of Trp residues based upon the  $\chi^2$  torsional angle:  $\beta 37$  Trp,  $\alpha 14$  and acceptor  $\beta_1 15$  Trp, and donor  $\beta_2 15$  Trp residues. Indeed, the W3 mode in the fibers' parent spectrum can be fit to three peaks occurring at 1550, 1559, and 1565  $\text{cm}^{-1}$  (Figure 6), consistent with the frequencies determined from the difference spectra (Figure 5). The magnitude of the observed shifts, however, is larger than that predicted from the empirical relationship determined by Harada and co-workers.<sup>49</sup> We suggest that the relatively high frequency of the W3 mode relative to the predicted value arises from both conformational and environmental effects. An earlier study had determined that the W3 frequency was sensitive to the environment, as it was measured at 1563  $\text{cm}^{-1}$  in cyclohexane and at 1557  $\text{cm}^{-1}$  in H<sub>2</sub>O.<sup>13</sup> A correlation with solvent donor or acceptor number was not observed however, and more recently, UVRR measurements of deuterated-Trp derivatives did not detect a sensitivity of the W3 frequency to H-bonding.<sup>47</sup> We suggest that the W3 frequency is slightly sensitive to the local environment but not to H-bonding at the indole nitrogen. Thus, the elevated W3 frequency observed in FmetHb S fibers (Figure 5) results from an increase in hydrophobicity of the local environment around  $\beta_2 15$  donor Trp residues.

The Trp residues in Hb S fibers appear to be in distinctly different environments, as indicated by the two bands observed for both the W17 (Figure 3, inset) and the W3 modes (Figure 5) in the F-R and F-T difference spectra. We suggest that the

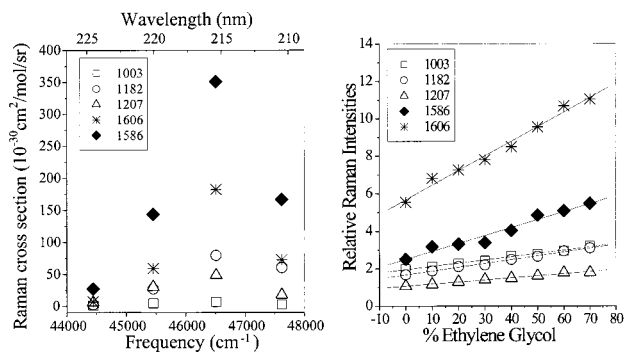


**Figure 7.** Raman excitation profiles of 1 mM Phe measured relative to 0.2 M  $\text{ClO}_4^-$  (left). Maximum enhancement of all Phe modes shown was observed at 215 nm. Relative intensity of Phe Raman bands in increasing concentrations of ethylene glycol (right). Spectra were obtained using an excitation wavelength of 215 nm. For all Phe modes, a linear increase in band intensity was observed with increasing ethylene glycol concentration.

two types of Trp residues observable in the UVRR difference spectra are the  $\beta 37$  Trp and the donor  $\beta 215$  Trp residues. The  $\alpha 14$  and acceptor  $\beta 115$  Trp residues are not significantly altered in going from tetramers to fibers and do not contribute to the F–T difference spectrum, as shown by the absence of a peak at  $1559 \text{ cm}^{-1}$ .

**UVRR Spectroscopy of Hb S Phe Residues: The Donor–Acceptor Interaction.** Phe residues were investigated using two excitation wavelengths, 210 and 215 nm. Although previous determination of Phe Raman cross sections was suggestive of a maximum at 210 nm excitation,<sup>48</sup> we find that 215 nm excitation optimally enhances the signal arising from all Phe bands observed and, most significantly, the F8b and F8a modes occurring at 1586 and  $1606 \text{ cm}^{-1}$  (Figure 7). This enhancement arises from excitation into the  $L_a$  transition band.<sup>48</sup> At this excitation wavelength, vibrational modes from the protein backbone and the Pro and His residues all contribute to the Raman spectrum. As enhancement of amide vibrational modes increases with shorter excitation wavelengths, a second excitation wavelength of 210 nm was used to clarify amide mode assignments.

The 215 nm-excited fiber and R-state tetramer spectra are dominated by Phe and Tyr vibrational modes (Figure 8). The majority of Phe and Tyr modes overlap in frequency because of the similarity in molecular geometry. The T–R difference spectrum obtained with 215 nm excitation is mainly composed of negative peaks and strongly resembles the difference spectra generated using 220 nm excitation.<sup>17,20</sup> In the high-frequency region, negative peaks occur at 1615, 1604, 1585, and  $1559 \text{ cm}^{-1}$ ; the peaks at 1615, 1604, and  $1585 \text{ cm}^{-1}$  are assigned to the  $\nu 8b$  and  $\nu 8a$  benzene-like ring-stretching modes of both Phe and Tyr residues. These bands are negative in the T–R difference spectrum because the Raman excitation profile of Tyr red shifts as a consequence of stronger H-bonding and hydrophobicity. The formation of the  $\alpha 42 \text{ Tyr} \cdots \beta 99 \text{ Asp}$  H-bond leads to a red shifting of the excitation profile and the observation of negative bands. At 210 nm, positive bands are observed at 1616, 1595, and  $1190 \text{ cm}^{-1}$  in the T–R difference spectrum (Figure 9). These bands can be assigned to Tyr residues, and the observed frequency upshift is consistent with  $\alpha 42$  H-bond formation. In a previous study, Tyr modes were observed to be positive in a T–R difference spectrum generated with 212 nm excitation.<sup>49</sup> The Raman-scattering cross section depends steeply on excitation wavelength, such that negative Tyr bands are observed at 218 and 215 nm, whereas positive Tyr bands are observed at 212 and 210 nm.

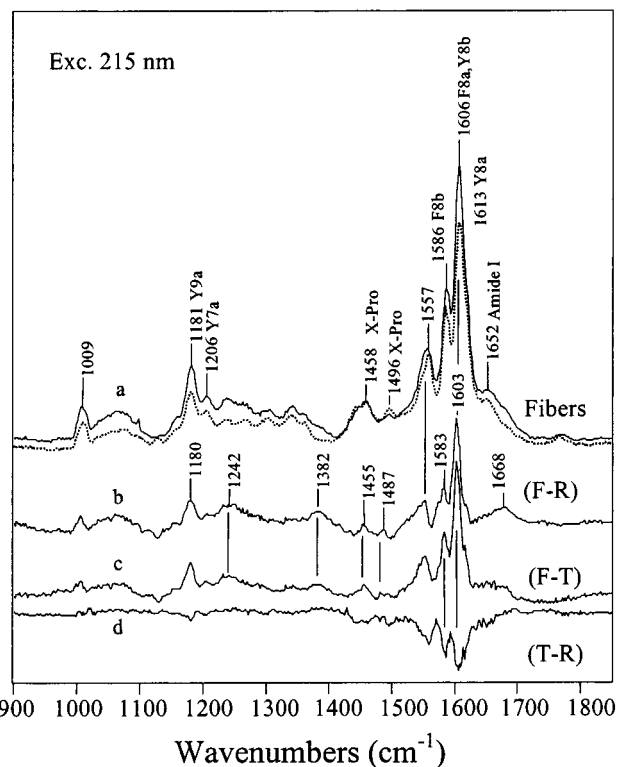


**Figure 8.** (a) UVRR spectra of FmetHb S fibers and R-state tetramers. (b) Difference spectrum generated between fibers and R-state tetramers (F–R). (c) Difference spectrum generated between fibers and T-state tetramers (F–T). (d) Difference spectrum generated between T- and R-state tetramers (T–R). All spectra were obtained with 215 nm excitation.

For Phe residues, it was previously determined using an excitation wavelength of 230 nm that the  $\nu_{12}$  mode occurring at  $1004 \text{ cm}^{-1}$  increases in intensity if the local environment becomes more hydrophobic.<sup>29</sup> We have extended that study to examine the effect of local environment on Phe signal intensity using excitation wavelengths of 215 and 210 nm (Figure 7). In the current work, ethylene glycol is used to simulate a protein interior or local hydrophobic environment. UVRR spectra of Phe solutions reveal that the signal intensity of Phe bands scales linearly with increasing ethylene glycol concentration. The 1586 (F8b) and  $1606 \text{ (F8b)} \text{ cm}^{-1}$  modes exhibit the steepest dependence on ethylene glycol concentration (Figure 7) and are expected to be most sensitive to any changes in local environment. From this intensity dependence on local environment, it can be inferred that the negative peaks observed at 1583 and  $1604 \text{ cm}^{-1}$  in the T–R spectrum arise from increased solvent exposure of one or more Phe residues. The 15 Phe residues contained in an  $\alpha\beta$  dimer all contribute to the observed Raman bands, making residue-specific mode assignments difficult. This spectral complexity is reduced in the T–R difference spectrum, which identifies only those residues that experience a change in environment upon conversion to the T-state. A possible candidate for the source of the Phe difference signals is the  $\beta 85$  Phe residue, located in the EF corner. An important lateral contact in Hb S fibers occurs in this region, which is thought to become more solvent exposed in the T-quaternary state. The increased exposure of this contact is thought to promote Hb S fiber formation.<sup>3</sup> Increased solvent exposure of  $\beta 85$  Phe in the T-state of unassociated tetramers would lead to a decrease in Raman intensity and negative bands in the difference spectrum. Interestingly, UVRR spectra of FmetHb A are suggestive that

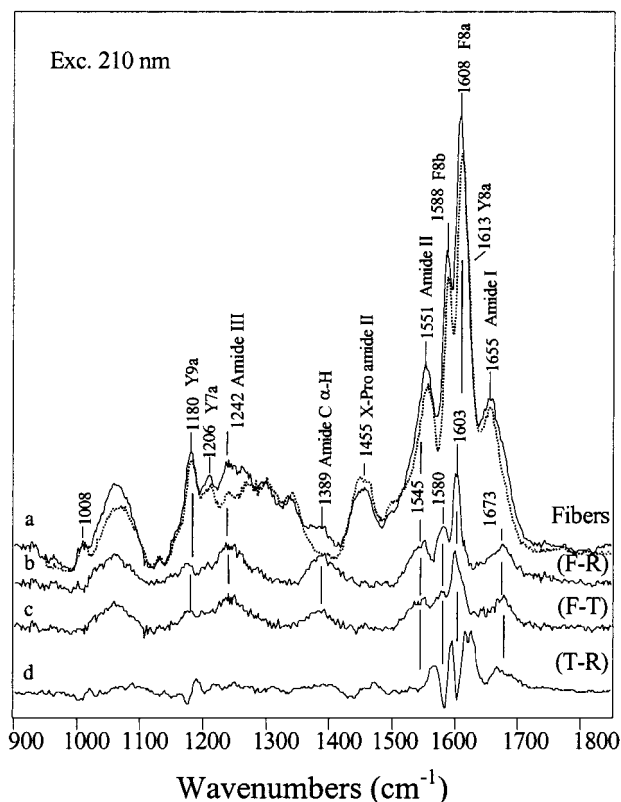


**Figure 9.** (a) UVRR spectra of FmetHb S fibers and R-state tetramers. (b) Difference spectrum generated between fibers and R-state tetramers (F–R). (c) Difference spectrum generated between fibers and T-state tetramers (F–T). (d) Difference spectrum generated between T- and R-state tetramers (T–R). All spectra were obtained with 210 nm excitation.

the relative exposure of the EF corner is greater in Hb S than in Hb A (data not shown).

The F–R and F–T difference spectra are distinctly changed from the T–R difference spectrum as a result of a profound increase in Phe signal intensity (Figure 8). The strongest positive bands occur at 1603 and 1583  $\text{cm}^{-1}$ , corresponding to the ring-stretching F8a and F8b modes. Other Phe modes occurring at 1006 (F12), 1207 (F7a), and 1180 (F9a)  $\text{cm}^{-1}$  also increase in intensity with fiber formation, as shown by positive peaks in the difference spectra. The intensity of these bands is not as sharply dependent on the local environment, as shown by their behavior with increasing ethylene glycol concentrations (Figure 7), and therefore, their contribution to the difference spectrum is not as pronounced as those of F8a and F8b. Positive F8a and F8b bands are also observed in the fibers' difference spectra generated with 210 nm excitation (Figure 9), although, in the T–R difference spectrum, they appear as negative bands. Phe signals are not as enhanced at this excitation wavelength (Figure 7), and consequently, the weaker Phe modes are not as prominent in the difference spectra. Nevertheless, the data obtained at 210 nm confirm the results obtained with 215 nm excitation and are indicative of a dramatic increase in Phe signal intensity upon fiber formation. The increased intensity of the Phe signal in fibers obscures any contribution from Tyr residues to the 210 and 215 nm excited F–R and F–T difference spectra.

Since the intensity of Phe Raman bands is sensitive to the local environment (see above), the positive Phe peaks observed in the F–R and F–T difference spectra are suggestive of an increase in hydrophobicity with fiber formation. As this effect is only associated with fiber formation and not with formation

of the T-state, we propose that the Phe signal increase arises from one or more of the axial and lateral contacts observed in the Hb S double strand. The most obvious and likely candidate is the lateral contact formed between the mutant  $^2\beta_26$  Val donor and the  $^1\beta_185$  Phe of the acceptor pocket (Figure 1).<sup>7</sup> This hydrophobic contact is believed to be the driving force for the association of tetramers into fibers. The other possibility is a nonpolar axial contact formed between the  $\alpha_2114$  Pro and  $\alpha_2115$  Ala of one tetramer and the  $\beta_1118$  Phe of a second tetramer. We cannot exclude the possibility that this contact also contributes to the increase in Phe signal intensity. Although the relative contribution of these two Phe residues to the F–R and F–T difference spectra cannot be separated without the use of mutants, we propose that the  $\beta_85$  Phe residue contributes substantially to the observed spectra, as the hydrophobicity of this contact is essential for Hb S fiber formation.<sup>1,2</sup> UVRR spectroscopy directly probes the relative hydrophobicity of the donor–acceptor interaction.

**UVRR Spectroscopy of Pro Residues.** Shorter excitation wavelengths also enhance contributions from other residues in the protein; the excitation wavelengths of 210 and 215 nm enhance the signal from Pro backbone residues. For the X–Pro bond, the  $\pi \rightarrow \pi^*$  electronic absorption transition of the peptide carbonyl is red shifted relative to protein backbone  $\pi \rightarrow \pi^*$  transitions because of the increased functionality of the Pro nitrogen. In a previous study of Hb A, X–Pro modes were observed in the T–R difference spectrum at 1464  $\text{cm}^{-1}$  and tentatively assigned to the  $\alpha_37$  Pro residue.<sup>49</sup> In the 210 nm-excited data of FmetHb S, a broad envelope is observed for the X–Pro amide II mode at 1450  $\text{cm}^{-1}$ , which yields a higher frequency peak at 1465  $\text{cm}^{-1}$  in the difference spectrum. In the fibers difference spectra of F–R and F–T, this mode occurs at 1455  $\text{cm}^{-1}$ , approximately 10  $\text{cm}^{-1}$  lower than that observed in the T–R spectrum. The frequency downshift is suggestive of a decrease in H-bond strength in the fibers relative to unassociated T-state tetramers, as stronger H-bond donation shifts the X–Pro amide II mode to a higher wavenumber.<sup>50,51</sup> The deoxy Hb A and deoxy Hb S X-ray crystal structures are suggestive of similar environments for the majority of Pro residues. Nevertheless, a possible source of the frequency downshift is the H-bond formed between the  $\beta_25$  Pro and the  $\beta_29$  Ser in the Hb S donor subunits, which is  $\sim 0.3$  Å longer than the same H-bond in deoxy Hb A.<sup>7,40</sup> This difference in length could lead to a substantial difference in the strength of the observed H-bond. In solution, both the increased disorder of the amino termini and the inherent plasticity of the donor–acceptor interaction may lead to a longer H-bond length and, consequently, lower frequency of the X–Pro amide II mode. Thus, analysis of the X-ray crystal structures is suggestive that the  $\beta_5$  Pro residue that is adjacent to the donor  $\beta_6$  Val is responsible for the Pro signal observed in the fibers' difference spectra.

**Secondary Structure Conformation Probed by UVRR Spectroscopy.** Amide vibrational modes arising from the protein backbone are diagnostic of protein conformation and can be used to quantify secondary structure elements.<sup>45,52</sup> These modes are enhanced by excitation into the  $\pi \rightarrow \pi^*$  transition of the peptide bond. The excitation wavelength of 210 nm occurs in the red edge of this absorption band; however, amide modes are sufficiently enhanced to be detectable in UVRR parent and difference spectra. In the T–R spectrum, no distinctive changes in the amide modes are observed (Figure 9). Two bands, observed at 1566 and 1667  $\text{cm}^{-1}$ , are of uncertain assignment and could arise from amide I and amide II. We note that other

amide vibrational modes, namely amide III and  $C_{\alpha}$ -H, are not detected, which is not consistent with assignment of the bands at 1566 and 1667  $\text{cm}^{-1}$  to amide I and II. We suggest that the mode at 1667  $\text{cm}^{-1}$  arises from Tyr residues, and possible assignments are to an overtone ( $2 \times Y10a$ ) or a combination ( $Y18a + Y6b$ ) band. This mode has been previously observed for the model compounds *p*-cresol<sup>53</sup> and *p*-ethylphenol,<sup>54</sup> and we argue that the improved signal-to-noise of our data allows us to observe this mode in difference spectra. The mode at 1565  $\text{cm}^{-1}$  was tentatively assigned to the W2 mode of Trp residues in a previous study;<sup>49</sup> however, in our 210 nm-excited spectra, the absence of other Trp modes argues against that assignment (Figure 9). We suggest that this mode arises from His residues which experience a change in conformation or protonation upon forming the T-state, as suggested earlier by Spiro and co-workers.<sup>49,55</sup> The 210 nm-excited T-R difference spectrum (Figure 9) shows no evidence of any changes in the intensity or frequency of amide modes, consistent with an absence of change in secondary structure.

Fiber formation leads to changes in the intensity and frequency of amide modes in both the parent and difference spectra obtained with 210 nm excitation (Figure 9). In the fiber spectrum, the amide I mode occurring at 1655  $\text{cm}^{-1}$  is noticeably broadened relative to the R-state spectrum, indicative of an increase in heterogeneity of the peptide backbone. In the difference spectra, positive peaks are observed at 1673, 1545, 1242, and 1387  $\text{cm}^{-1}$ , which can be assigned to amide modes, I, II, III, and  $C_{\alpha}$ -H, respectively. The observation of positive peaks is consistent with a loss of  $\alpha$ -helical structure, as the formation of  $\alpha$ -helices and the associated absorption hypochromism is manifested as a suppression of amide band intensity in UVRR spectra.<sup>45</sup> Thus, the intensity increase of amide II and amide  $C_{\alpha}$ -H at 1545 and 1389  $\text{cm}^{-1}$  is consistent with a loss of helical structure. The frequency and width of the amide I and III modes are diagnostic of secondary structure type and can be used to identify the changes in secondary structure in FmetHb S fibers. The relatively high frequency of the amide I band (1673  $\text{cm}^{-1}$ ) and the low frequency of amide III (1242  $\text{cm}^{-1}$ ) are indicative of an increase in unordered or random secondary structure conformation.<sup>45,52</sup> This observation is in keeping with the X-ray crystal structure of deoxy Hb S, in which the amino termini of the  $\beta$  subunits were found to be relatively disordered, with high-temperature factors and relatively little electron density observed for the first three residues.<sup>7</sup> We suggest that the increase in random protein conformation observed by UVRR spectroscopy is consistent with the increased disorder of the amino termini of the  $\beta$  subunits found in the X-ray crystal structure.

## Conclusion

In conclusion, we observe that UVRR spectroscopy is a sensitive probe of FmetHb S fibers. A comparison of spectra obtained with fibers and unassociated tetramers reveals that UVRR is sensitive to many of the structural changes occurring in fibers. These structural details of the fibers, which confirm many of those observed by X-ray crystallography, help to establish that the basic building block of Hb S fibers in solution is the Wishner-Love double strand. In particular, the dramatic increase in Phe signal intensity is attributed to an increase in hydrophobicity of the local environment, as would be predicted from the important lateral contact formed between the mutant  $\beta_26$  Val and the hydrophobic pocket formed by  $\beta_185$  Phe and  $\beta_188$  Leu (Figure 1). Trp residues also exhibit spectral characteristics consistent with an extremely hydrophobic environment;

heterogeneity of the W3 mode coupled with the structural data supports the assignment of the increased hydrophobicity to donor  $\beta_215$  and not acceptor  $\beta_115$  residues. Most significantly, the Raman data reveal that the  $\alpha_1\beta_2$  intersubunit contacts are stronger in the fibers than in unassociated tetramers. This finding, which is not necessarily predicted from the X-ray crystal structure, is consistent with the observation that Hb S fibers exhibit a much lower ligand binding affinity and rate of ligand binding relative to T-state tetramers. Consequently, we suggest that UVRR spectroscopy provides new insight into the structure of Hb S fibers and will be a useful tool for further probing the mechanism of fiber formation.

**Acknowledgment.** We are grateful to Dr. Kenneth Bridges of Brigham and Women's Hospital for providing us with sickle cell blood. We thank Marielle Yohe, Shar-yin Naomi Huang, and Keating Van Dorsten for their assistance in isolating sickle cell hemoglobin. We are grateful to Daniel Coman for the spectra of Phe in ethylene glycol. This work was supported by an American Heart Association Grant in Aid (GA 96015120).

## References and Notes

- (1) Padlan, E. A.; Love, W. E. *J. Biol. Chem.* **1985**, *260*, 8280–8291.
- (2) Padlan, E. A.; Love, W. E. *J. Biol. Chem.* **1985**, *260*, 8272–8279.
- (3) Dickerson, R.; Geis, I. *Hemoglobin: Structure, Function, Evolution and Pathology*; Benjamin Cummins: Menlo Park, 1983.
- (4) Wellemans, T. E.; Josephs, R. *J. Mol. Biol.* **1979**, *135*, 651–674.
- (5) Watowich, S.; Gross, L.; Josephs, R. *J. Struct. Biol.* **1993**, *111*, 161–179.
- (6) Cretegy, I.; Edelstein, S. *J. Mol. Biol.* **1993**, *230*, 733–738.
- (7) Harrington, D. J.; Adachi, K.; Royer, W. E., Jr. *J. Mol. Biol.* **1997**, *272*, 398–407.
- (8) Briehl, R. *J. Mol. Biol.* **1995**, *245*, 710–723.
- (9) Briehl, R. W.; Mann, E. S.; Josephs, R. *J. Mol. Biol.* **1990**, *211*, 693–698.
- (10) Wishner, B. C.; Ward, K. B.; Lattman, E. E.; Love, W. E. *J. Mol. Biol.* **1975**, *98*, 179–194.
- (11) Benesch, R.; Kwong, S.; Benesch, R. *Nature* **1982**, *299*, 231–234.
- (12) Nagel, R. L.; Bookchin, R. M. In *Biological and Clinical Aspects of Hemoglobin Abnormalities*; Caughey, W. S., Ed.; Academic Press: New York, 1978; pp 195–201.
- (13) Rodgers, K.; Su, C.; Subramaniam, S.; Spiro, T. *J. Am. Chem. Soc.* **1992**, *114*, 3697–3709.
- (14) Jayaraman, V.; Rodgers, K. R.; Mukerji, I.; Spiro, T. G. *Science* **1995**, *269*, 1843–1848.
- (15) Kitagawa, T. *Prog. Biophys. Mol. Biol.* **1992**, *58*, 1–18.
- (16) Huang, J.; Juszczak, L. J.; Peterson, E. S.; Shannon, C. F.; Yang, M.; Huang, S.; Vidugiris, G. V. A.; Friedman, J. M. *Biochemistry* **1999**, *38*, 4514–4525.
- (17) Jayaraman, V.; Rodgers, K. R.; Mukerji, I.; Spiro, T. G. *Biochemistry* **1993**, *32*, 4547–4551.
- (18) Mukerji, I.; Spiro, T. G. *Biochemistry* **1994**, *33*, 13132–13139.
- (19) Huang, S.; Peterson, E. S.; Ho, C.; Friedman, J. M. *Biochemistry* **1997**, *36*, 6197–6206.
- (20) Sokolov, L.; Mukerji, I. *J. Phys. Chem. B* **1998**, *102*, 8314–8319.
- (21) Juszczak, L. J.; Hirsch, R. E.; Nagel, R. L.; Friedman, J. M. *J. Raman Spectrosc.* **1998**, *29*, 963–968.
- (22) Perutz, M. F.; Heidner, E. J.; Ladner, J. E.; Beetlestone, J. G.; Ho, C.; Slade, E. F. *Biochemistry* **1974**, *13*, 2187–2200.
- (23) Yohe, M. E.; Sheffield, K. M.; Mukerji, I. *Biophys. J.* **2000**, *78*, 3218–3226.
- (24) Harrington, D. J.; Adachi, K.; Royer, W. E., Jr. *J. Biol. Chem.* **1998**, *273*, 32690–32696.
- (25) Adachi, K.; Konitzer, P.; Kim, J.; Welch, N.; Surrey, S. *J. Biol. Chem.* **1993**, *268*, 21650–21656.
- (26) Adachi, K.; Reddy, L. R.; Surrey, S. *J. Biol. Chem.* **1994a**, *269*, 31563–31566.
- (27) Adachi, K.; Konitzer, P.; Paulraj, C.; Surrey, S. *J. Biol. Chem.* **1994b**, *269*, 17477–17480.
- (28) Reddy, L. R.; Reddy, K. S.; Surrey, S.; Adachi, K. *J. Biol. Chem.* **1996**, *271*, 24564–24568.
- (29) Hildebrandt, P.; Copeland, R.; Spiro, T.; Otlewski, J.; Laskowski, M.; Prendergast, F. *Biochemistry* **1988**, *27*, 5426–5433.
- (30) Shapiro, D. B.; Esquerra, R. M.; Goldbeck, R. A.; Ballas, S. K.; Mohandas, N.; Kliger, D. S. *J. Biol. Chem.* **1995**, *270*, 26078–26085.

- (31) Sunshine, H.; Hofrichter, J.; Ferrone, F.; Eaton, W. *J. Mol. Biol.* **1982**, *158*, 251–273.
- (32) Antonini, E.; Brunori, M. *Hemoglobin and Myoglobin and Their Reactions with Ligands*; North-Holland Publishing Company: London, 1971.
- (33) Huisman, T. H. J.; Dozy, A. M. *J. Chromatogr.* **1965**, *19*, 160–169.
- (34) Di Iorio, E. *Methods Enzymol.* **1981**, *76*, 57–72.
- (35) Mukerji, I.; Sokolov, L.; Mihailescu, M.-R. *Biopolymers* **1998**, *46*, 475–487.
- (36) Hu, X.; Spiro, T. G. *Biochemistry* **1997**, *36*, 15701–15712.
- (37) Nagai, M.; Wajcman, H.; Lahary, A.; Nakatsukasa, T.; Nagatomo, S.; Kitagawa, T. *Biochemistry* **1999**, *38*, 1243–1251.
- (38) Wang, D.; Spiro, T. G. *Biochemistry* **1998**, *37*, 9940–9951.
- (39) Hu, X.; Dick, L. A.; Spiro, T. G. *Biochemistry* **1998**, *37*, 9445–9448.
- (40) Fermi, G.; Perutz, M. F.; Shanaan, B.; Fourme, R. *J. Mol. Biol.* **1984**, *175*, 159.
- (41) Miura, T.; Takeuchi, H.; Harada, I. *J. Raman Spectrosc.* **1989**, *20*, 667.
- (42) Miura, T.; Takeuchi, H.; Harada, I. *Biochemistry* **1988**, *27*, 88–94.
- (43) Harada, I.; Takeuchi, H. In *Spectroscopy of Biological Systems*; Clark, R. J. H., Hester, R. E., Eds.; Wiley: New York, 1986; pp 113–175.
- (44) Harada, I.; Miura, T.; Takeuchi, H. *Spectrochim. Acta* **1986**, *42A*, 307–312.
- (45) Austin, J. C.; Jordan, T.; Spiro, T. G. In *Biomolecular Spectroscopy*; Clark, R. J. H., Hester, R. E., Eds.; Wiley: New York, 1993; pp 55–127.
- (46) Hashimoto, S.; Obata, K.; Takeuchi, H.; Needleman, R.; Lanyi, J. K. *Biochemistry* **1997**, *36*, 11583–11590.
- (47) Maruyama, T.; Takeuchi, H. *J. Raman Spectrosc.* **1998**, *26*, 319–324.
- (48) Fodor, S.; Copeland, R.; Grygon, C.; Spiro, T. *J. Am. Chem. Soc.* **1989**, *111*, 5509–5518.
- (49) Zhao, X.; Spiro, T. G. *J. Raman Spectrosc.* **1998**, *29*, 49–55.
- (50) Jordan, T.; Mukerji, I.; Wang, Y.; Spiro, T. G. *J. Mol. Struct.* **1996**, *379*, 51–64.
- (51) Harada, I.; Takeuchi, H. *J. Raman Spectrosc.* **1990**, *21*, 509.
- (52) Chi, Z.; Chen, X. G.; Holtz, J. S. W.; Asher, S. A. *Biochemistry* **1998**, *37*, 2854–2864.
- (53) Takeuchi, H.; Watanabe, N.; Harada, I. *Spectrochim. Acta* **1988**, *44A*, 749–761.
- (54) Russell, M. P.; Vohnik, S.; Thomas, G. J., Jr. *Biophys. J.* **1995**, *68*, 1607–1612.
- (55) Zhao, X.; Wang, D.; Spiro, T. G. *J. Am. Chem. Soc.* **1998**, *120*, 8517–8518.